Higher-order- and multimode properties of nonlinear multipass cells for temporal compression

Marc Hanna, Michele Natile, Florent Guichard, Gautier Parize, Xavier Délen, Patrick Georges

Research Article Vol. 42, No. 3 / March 2025 / Journal of the Optical Society of America B 631

Journal of the Optical Society of America B

OPTICAL PHYSICS

Higher-order- and multimode properties of nonlinear multipass cells for temporal compression

Marc Hanna,[1,*] Michele Natile,[2] Florent Guichard,[2] Gautier Parize,[1,2] Xavier Délen,[1] and Patrick Georges[1]

[1]Université Paris-Saclay, Institut d'Optique Graduate School, CNRS, Laboratoire Charles Fabry, 91127 Palaiseau, France
[2]Amplitude, 11 Avenue de Canteranne, Cité de la Photonique, 33600 Pessac, France
*marc.hanna@institutoptique.fr

Received 3 September 2024; revised 17 December 2024; accepted 10 January 2025; posted 10 January 2025; published 24 February 2025

Over the last few years, temporal compression in nonlinear multipass cells (MPCs) has been proven to be a very promising method for future ultrafast laser sources. Although the majority of the work has been done with Gaussian beams, a few studies have touched upon using structured beams in such subsystems. Here, based on coupled-mode theory and numerical simulations, we focus on the behavior of MPCs upon excitation with either a single higher-order spatial mode or a combination of such modes. This includes their nonlinear properties, linear spatial dynamics upon propagation, and selection rules for efficient nonlinear energy transfer between modes. In particular, we show that the use of high-angular-order Laguerre–Gauss modes should prove efficient to scale the pulse energy inside MPCs.

https://doi.org/10.1364/JOSAB.540948

1. INTRODUCTION

Since the first demonstration [1], multipass cells (MPCs) have become, over the last few years, one of the preferred platforms for nonlinear temporal compression [2,3] and are starting to be used for other nonlinear optics phenomena such as contrast enhancement [4] and Raman conversion [5]. One of their main features is the robustness of their spatial properties in the presence of significant accumulated nonlinearity: When excited with a Gaussian beam, the output beam remains Gaussian, and spectral/temporal properties are modified by the nonlinearity homogeneously across the spatial beam profile. This peculiar property was elucidated using coupled-mode theory well before the appearance of nonlinear MPCs [6] and is related to the fact that the Gouy phase inhibits nonlinear energy transfer between the Gaussian beam and higher-order modes.

Beyond this remarkable property, the spatial dynamics inside MPCs has not been investigated in detail. Among the few studies, oscillatory deviations in beam size from the stationary beam caused by Kerr lensing were investigated, leading to the concept of nonlinear mode matching [7,8]. The suppression of small-scale self-focusing in a bulk material-based MPC compared to single-stage spectral broadening was examined [9]. Most experiments and numerical simulations of nonlinear pulse propagation of MPCs have been performed with linearly polarized Gaussian beams, with a few notable exceptions. For instance, the propagation of radially and azimuthally polarized beams in MPCs was studied with simulations [10]. The same authors also proposed to perform nonlinear compression with vortex beams, backed by numerical simulations [11], in view of generating very short, quasi-single-cycle vortex beams. The experimental demonstration that energy scaling of temporal compression in an MPC is possible using a first-order vortex beam was achieved at an unprecedented pulse energy level of 100 mJ [12]. More generally, the recent blooming of multimode nonlinear optics [13], including several pulse compression experiments inside gas-filled capillaries [14–16], motivates the investigation of the behavior of nonlinear MPCs with respect to structured light composed of a higher-order- or multimode input beam.

In this work, we examine the multimode spatial dynamics inside gas-filled MPCs, in both linear and nonlinear regimes. We first establish their linear reimaging properties, similar to graded-index multimode fibers [17]. We then study the nonlinear regime using both arguments from the coupled-mode theory and full numerical simulations. This allows us to derive selection rules for significant energy transfer among modes. The scaling of nonlinear properties of higher-order modes is also recapitulated to examine their potential for energy scaling. These considerations are validated with the simple case of a Gaussian input beam and then extended with a single higher-order mode excitation.

Finally, we examine the case where a set of modes is used as the initial condition to nonlinear propagation of the MPC. One of the main results of this work is that the single higher-order mode excitation is stable upon nonlinear propagation, providing a way for energy scaling beyond the first-order vortex mode.

2. SELF-REIMAGING PROPERTIES OF MPCs IN THE LINEAR REGIME

We use decomposition of the input field upon the Laguerre–Gauss modes, which provide a complete basis for solutions of the linear paraxial propagation equation in freespace, well suited to beams with a radial symmetry. Nonlinearity will be considered as a perturbation that causes both energy transfer among these modes and amplitude-dependent dephasing effects. These modes are given by

$$\mathrm{LG}_{\ell p}(r,\theta,z)=\sqrt{\frac{2}{\pi}}\frac{C_{\ell p}}{w(z)}\left(\frac{\sqrt{2}r}{w(z)}\right)^{|\ell|}L_p^{|\ell|}\left(\frac{2r^2}{w(z)^2}\right)\times\exp\left\{-\frac{r^2}{w^2(z)}-j\left[\frac{\beta_0 r^2}{2R(z)}+\ell\theta-\psi_{\ell p}(z)\right]\right\}, \tag{1}$$

where ℓ, p are the angular and radial mode numbers, $L_p^{|\ell|}$ is the generalized Laguerre polynomial, w_0 is the beam radius at the waist, $z_R=\pi w_0^2/\lambda_0$ is the Rayleigh range, λ_0 is the central wavelength, and β_0 is the wave number. The beam radius, radius of curvature, and Gouy phase evolve along z according to $w^2(z)=w_0^2(1+z^2/z_R^2)$, $R(z)=z(1+z_R^2/z^2)$, and $\psi_{\ell p}(z)=(1+2p+|l|)\arctan(z/z_R)$. We will refer to $(1+2p+|l|)$ as the Gouy phase multiplier since this quantity plays an important role in the phase-matching condition that governs efficient energy transfer among modes. These modes are normalized so that $\int_A|\mathrm{LG}_{\ell p}|^2dA=1$ through the constant $C_{\ell p}=\sqrt{p!/(p+|\ell|)!}$.

In a mode-matched MPC, the beam is periodically refocused by two curved mirrors facing each other through a waist, and therefore each mode experiences a Gouy phase at each pass. The Gouy phase acquired by mode $\mathrm{LG}_{\ell p}$ over a single pass in the MPC is given as [3]

$$\psi_{\ell p}^{\mathrm{SP}}=2(1+2p+|l|)\arctan\left(\frac{C}{\sqrt{C(2-C)}}\right), \tag{2}$$

where $C=L/R$, L is the MPC length, and R is the radius of curvature of the mirrors, as shown in Fig. 1. In a graded-index multimode fiber, the equal spacing of the propagation constants results in periodic reimaging of the input spatial intensity pattern [17]. In analogy to this, in an MPC, the differential phase accumulated between modes at each single pass is an integer multiple of twice the arctan term. Periodic reimaging occurs when the cumulated differential phase is equal to $2k\pi$, with k being an integer, corresponding to a number of passes equal to

$$N_{\mathrm{SP}}=\frac{k\pi}{\arctan\left(\frac{C}{\sqrt{C(2-C)}}\right)}. \tag{3}$$

For quasi-concentric MPCs ($L\to 2R$), the differential phase acquired upon propagation over a single pass is slightly less than π, and N_{SP} is a noninteger and slightly larger than 2 for $k=1$. Reimaging occurs at a periodicity that is just over one roundtrip. For other geometries such as quasi-confocal ($L\approx R$) or quasi-collimated ($L\ll R$), the reimaging period is around two roundtrips (single-pass differential phase $\approx\pi/2$) and much greater than a roundtrip (single-pass differential phase $\ll\pi$), respectively.

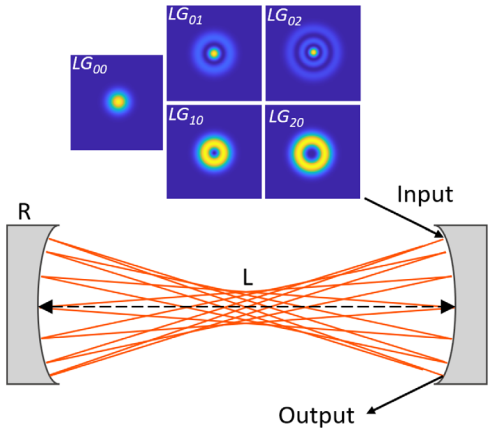

Fig. 1. Schematic of the MPC, showing the intensity profile of the first few LG modes.

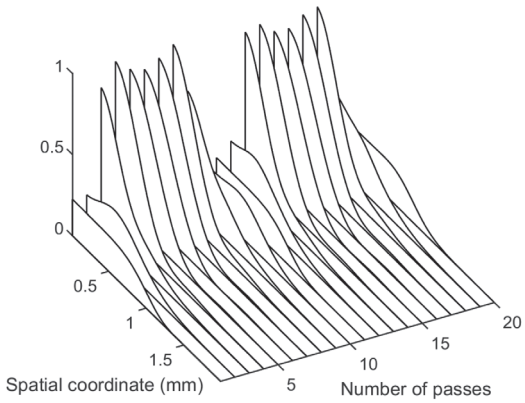

Fig. 2. Intensity profile as a function of number of passes for a flat-top input beam in linear conditions.

Reimaging at the cell mirror occurs if N_{SP} is an integer for a certain value of k. It can be easily shown that this condition obtained from considerations on the Gouy phase corresponds to the ray-optics imaging condition obtained for this periodic system using an ABCD matrix formalism [18]. The prototype quasi-concentric MPC configuration we choose for this study is $R=300$ mm and $L=585.3$ mm, which results in reimaging at the cell mirror after 20 passes. To test this against our numerical simulations model, we run it in linear condition, with a flat-top super-Gaussian input spatial profile exhibiting no orbital angular momentum (OAM). This input condition can be decomposed over LG_{0p} modes. The resulting intensity profiles after each of the 20 passes are shown in Fig. 2. Dephasing among modes causes the intensity profile to evolve upon propagation, but we observe reimaging after 10 and 20 passes as expected. This reimaging period is halved compared to Eq. (3) because of the factor of 2 that appears in the Gouy phase multiplier for LG_{0p} modes.

In the presence of nonlinearity, this self-reimaging behavior is perturbed by energy exchange among modes and nonlinear self- and cross-phase modulation (SPM and XPM). We now examine the nonlinear properties of Laguerre–Gaussian modes.

3. NONLINEAR PROPERTIES OF LAGUERRE–GAUSSIAN MODES

Several parameters are important when considering the design of nonlinear MPCs with higher-order modes. First, the effective area determines the rate at which the instantaneous optical power in a given mode translates into the accumulation of nonlinear phase as a result of SPM. It, therefore, determines the amount of B-integral experienced by the beam as it propagates in the MPC. This area is given by

$$A_{\ell p}^{\text{eff}} = \frac{\left(\int_A |\text{LG}_{\ell p}|^2 \text{d}A\right)^2}{\int_A |\text{LG}_{\ell p}|^4 \text{d}A}. \tag{4}$$

Evaluation of this integral shows that the effective area of higher-order $\text{LG}_{\ell p}$ modes is proportional to that of the Gaussian mode along propagation, and Table 1 shows this proportionality constant for the first three LG_{0p} and $\text{LG}_{\ell 0}$ modes. As the mode order increases, the amount of nonlinearity decreases at a given power, which could be problematic to reach a given temporal compression ratio. The expression for the B-integral per round-trip that was established for the Gaussian beam [19] can be used for $\text{LG}_{\ell p}$ modes, provided that it is divided by the correction factor shown in Table 1.

Since the peak power value inside the MPC can be limited by catastrophic self-focusing, it is also important to determine the critical power of the higher-order modes. This has been established recently [20], and critical power values for the same set of modes are also reported in Table 1. This critical power increases faster than the effective area with the mode orders, which should allow larger compression ratios when higher-order modes are used, since the B-integral per roundtrip can be limited by the critical power value. Finally, a third important parameter is the maximum intensity for a given peak power. It can be easily shown that this quantity is given by [21,22]

$$I_{\text{peak}}/I_{\text{peak0}} = \frac{|\ell|^{|\ell|} e^{-|\ell|}}{|\ell|!}. \tag{5}$$

As a result, increasing the radial mode order p does not provide any decrease in the peak intensity, while increasing the angular order ℓ is favorable since it allows us to increase the pulse energy while keeping the intensity at the value that is limited either by the ionization threshold at the focus or by the damage fluence on the mirrors [19]. These considerations are useful and necessary to determine the potential of using higher-order modes in MPCs, but they are not sufficient. Indeed, as recalled in Section 1, the essential feature of nonlinear MPCs is that the Gaussian beam shape is maintained upon nonlinear propagation, and the question arises whether or not this is true for single higher-order modes or combinations thereof.

Table 1. Nonlinear Properties of Some LG Modes[a]

	$A_{\text{eff}}/A_{\text{eff0}}$	$P_{\text{crit}}/P_{\text{crit0}}$	$I_{\text{peak}}/I_{\text{peak0}}$
LG_{00}	1	1	1
LG_{01}	2	6	1
LG_{02}	32/11	160/11	1
LG_{03}	64/17	448/17	1
LG_{10}	2	4	$1/e$
LG_{20}	8/3	8	$2/e^2$
LG_{30}	16/5	64/5	$27/(6e^3)$

[a] $A_{\text{eff0}} = \pi w^2(z)$, $P_{\text{crit0}} = 0.148\lambda^2/nn_2$, and $I_{\text{peak0}} = 2P/(\pi w^2(z))$ are the effective area, critical power, and peak intensity of the Gaussian beam, respectively, where n and n_2 are the linear and nonlinear refractive indices of the medium, respectively.

4. COUPLED-MODE THEORY

In order to address the stability of more general spatial excitations of MPCs, we use arguments derived from coupled-mode theory to examine the possibility of efficient energy transfer among modes. We first quickly recall its framework that was used both to gain insights into nonlinear freespace [6,22] and guided [23] propagation. The field propagating inside the MPC is decomposed into the LG mode basis as follows:

$$A(r, \theta, z, t) = \sum_{\ell p} A_{\ell p}(z, t)\text{LG}_{\ell p}(r, \theta, z). \tag{6}$$

By substituting this decomposition into the nonlinear propagation equation (neglecting self-steepening and wavelength-dependent diffraction) and projecting it onto the mode basis, a set of coupled nonlinear equations can be obtained for the mode amplitudes,

$$\left(\frac{\partial}{\partial z} - j\hat{D}\right) A_{\ell p} = j\gamma \sum_{\ell_1 p_1, \ell_2 p_2, \ell_3 p_3} \kappa_{\ell p, \ell_1 p_1, \ell_2 p_2, \ell_3 p_3} A_{\ell_1 p_1} A^*_{\ell_2 p_2} A_{\ell_3 p_3}, \tag{7}$$

where the dispersion operator $\hat{D} = \sum_{k=2}^{\infty} \beta_k/k!(j\partial/\partial z)$, $\beta_k = (\partial^k \beta/\partial \omega^k)_{\omega_0}$, the propagation constant $\beta(\omega) = n(\omega)\omega/c$, $n(\omega)$ is the refractive index of the gas, and the equation is written in the coordinate frame moving at the group velocity at the central wavelength. The nonlinear coefficient is given by $\gamma = n_2\omega_0/(\pi w_0^2)$. The coupling coefficients determine the nonlinear source terms and are given by

$$\kappa_{\ell p, \ell_1 p_1, \ell_2 p_2, \ell_3 p_3} = \pi w_0^2 \int_A \text{LG}_{\ell_1 p_1} \text{LG}^*_{\ell_2 p_2} \text{LG}_{\ell_3 p_3} \text{LG}^*_{\ell p} \text{d}A. \tag{8}$$

For a single mode, the self-coupling coefficient $\kappa_{\ell p, \ell p, \ell p, \ell p} = \pi w_0^2/A_{\ell p}^{\text{eff}}$, the inverse of the coefficient reported in Table 1, and we recover the fact that the spatially averaged nonlinear phase is accumulated at a rate given by the inverse of the effective area. Using symmetry arguments, and inspecting Eq. (8), it is easy to show that, if a single-mode ℓp is excited at the input, the coupling coefficients $\kappa_{\ell' p', \ell p, \ell p, \ell p}$ evaluate to zero if $\ell' \neq \ell$. This property relates to the topological protection of OAM modes or to the conservation law of OAM. As a result, the only modes that can gather energy from the input mode are the $\ell p'$ modes. However, for the energy transfer to be efficient, another condition to be met is that the Gouy phase multiplier of the nonlinear coefficient must be equal to zero. Indeed, if it is not

the case, source terms from longitudinal positions located at the same distance on opposing sides of the waist cancel out. This property is well known in the context of harmonic generation [24] and also leads to the explanation of the stability of Gaussian beams in the MPCs [6]. The Gouy phase multipliers of the nonlinear coupling coefficients are given by

$$\Psi\left[\kappa_{\ell p,\ell_1 p_1,\ell_2 p_2,\ell_3 p_3}\right] = (\ell_1 - \ell_2 + \ell_3 - \ell) + 2(p_1 - p_2 + p_3 - p). \quad (9)$$

As a result, if a single mode is excited at the input of the MPC, coupling to a mode with a different mode order ℓ is prohibited because the coupling coefficient is zero. Furthermore, for modes with the same angular order, coupling to a mode with a different radial order p is prohibited because the coupling coefficient does not have a zero Gouy phase multiplier: The ℓ contribution is zero and cannot compensate for the nonzero p contribution. In this case, the inhibition of coupling is not as strict, and a residual fraction of the energy can still be coupled to different radial order modes [6,22]. Overall, the use of a single higher-order mode should, therefore, result in stable propagation, even in the presence of significant Kerr effects. The next section is devoted to verifying this property using numerical simulations.

5. SINGLE HIGHER-ORDER MODE FOR TEMPORAL COMPRESSION

The numerical simulations used throughout this work are based on solving the generalized envelope propagation equation using the split-step method. We use a (2 + 1)D Hankel transform-based algorithm to model situations, where only LG_{0p} modes are involved. Indeed, in this case, the physical problem is radially symmetric, and removing one transverse dimension significantly reduces the computation time. In other cases, a full (3 + 1)D Fourier transform-based algorithm is used. We thoroughly checked that both models' results are identical. The physical effects taken into account are diffraction, including its wavelength dependence, all orders of chromatic dispersion, and all Kerr-based effects including SPM, XPM, intermodal four-wave mixing (FWM), Kerr lensing, and self-steepening. Most experiments are done in a regime where ionization plays a negligible role, because its onset leads to very unstable outputs; we therefore chose input parameters that do not require its inclusion in the model. The propagation equation is solved in the direct and reciprocal spaces, and no modal decomposition is used to compute the propagation. However, the field is projected onto a selected number of LG modes along the propagation, with a waist position and location that correspond to the perfect stationary Gaussian beam in the linear regime. We can observe the energy that is contained in nonmonitored modes by comparing the sum of the energy projected onto the monitored modes and the total energy contained in the propagated field.

A. Quasi-Concentric Cell

To validate the model and gain some insight on a simple case, we first model a benchmark case with the following parameters: the same quasi-concentric configuration is used as in Section 2 with $R = 300$ mm and $L = 585.3$ mm, there are 10 roundtrips, the MPC is filled with 5 bar of argon, and the mirrors do not introduce any spectral phase, with a reflectivity of 99.9%. The input pulse is Gaussian in both space and time, with a pulsewidth of 500 fs and an energy of 500 μJ, and is perfectly mode-matched to the linear stationary beam.

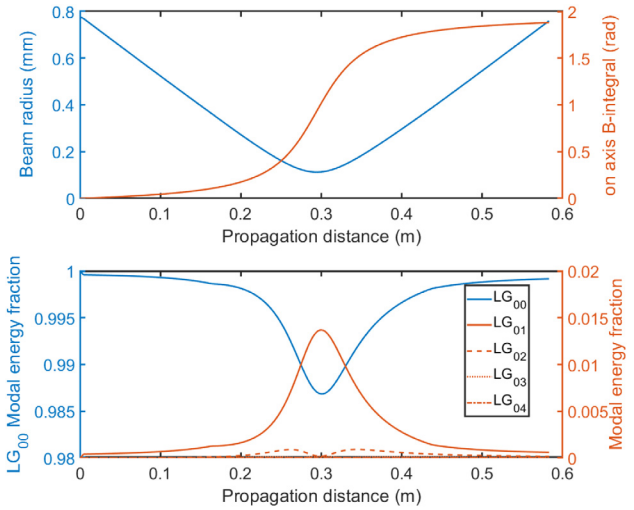

Fig. 3. (Top) Caustic and accumulated on-axis B-integral as a function of distance over the first pass for the concentric MPC driven by a Gaussian beam. (Bottom) Energy fraction in the LG_{0n} modes.

We first focus on the first pass to examine how the energy flows from the initially excited Gaussian mode to higher-order modes upon propagation through the waist. Figure 3 shows the evolution of the beam radius, on-axis (maximum, not spatially averaged) B-integral, and modal decomposition as a function of distance along this first pass. The effect identified in Ref. [6] is clearly visible: The energy fraction coupled into the mode with the highest coupling coefficient amplitude and the lowest Gouy phase multiplier of 2, LG_{01}, increases up to 1.5% at the waist and flows back to the LG_{00} mode in the remainder of the single-pass propagation. It is also interesting to observe that a lower energy fraction is coupled to the LG_{02} mode, both because of the lower magnitude of the coupling coefficient ($\kappa_{0p,00,00,00}$ scales as $1/2^p$ [6]) and because its Gouy phase multiplier is higher. As a result, the energy flows back and forth from LG_{00} to LG_{02} twice over the single pass.

Results obtained from this simulation after full propagation through 10 roundtrips are shown in Fig. 4. Overall, the energy remains in the spatial Gaussian mode. Small oscillations of the energy coupled to the LG_{01} mode are observed but can be traced back to the Kerr lens-induced oscillations of the beam size: The linear basis used for decomposition is slightly detuned from the actual beam size induced by nonlinearity. The time-resolved modal decomposition at the output also shows very limited power transfer to higher-order mode (99.6% of the output energy is in the Gaussian mode), but the small power fraction coupled to LG_{01} is interestingly located at time instants symmetrically away from the pulse maximum. The spectral broadening imparted by propagation corresponds to an output pulsewidth of 45 fs after introducing a group delay dispersion of -4600 fs^2, giving a compression ratio of 11.

Similar simulations were performed with an input beam in LG_{01} and LG_{02} modes and showed very similar behavior, in the

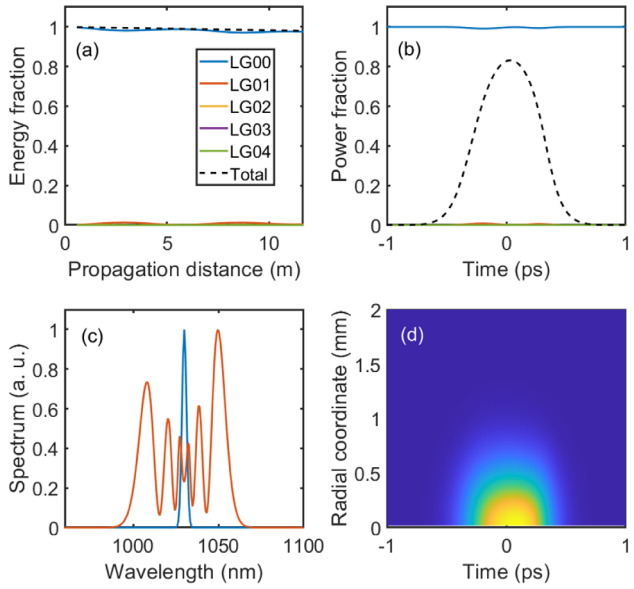

Fig. 4. (a) Modal content as a function of propagation distance in the quasi-concentric MPC excited with a Gaussian beam. (b) Time-resolved modal content at the output. The dashed line indicates the normalized space-averaged temporal profile at the output. (c) Input (blue) and output (red) spatially averaged spectra. (d) Output spatio-temporal intensity.

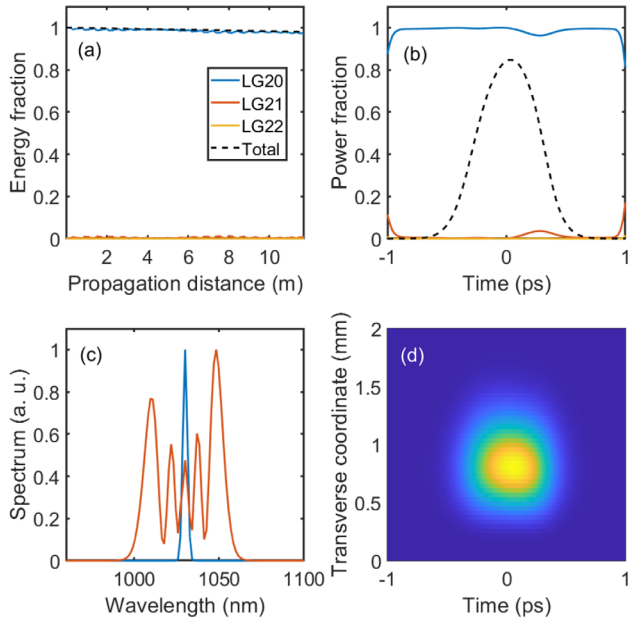

Fig. 5. (a) Modal content as a function of propagation distance in the quasi-concentric MPC excited with a LG_{20} mode. (b) Time-resolved modal content at the output. The dashed line indicates the normalized space-averaged temporal profile at the output. (c) Input (blue) and output (red) spatially averaged spectra. (d) Output spatio-temporal intensity.

sense that the energy fraction coupled to other modes remains small over propagation. To achieve the same spectral broadening, the input energy is increased to 1 mJ for the LG_{01} mode and 1.5 mJ for the LG_{02} mode in these simulations, consistent with the effective areas given in Table 1. The fraction of the output energy in the input mode is 98.5% in the LG_{01} case and 96.5% in the LG_{02} case. This slight degradation of the mode conservation could be related to the higher peak intensity necessary to keep the B-integral constant. Anyway, due to this very fact that the peak intensity at a given power is the same for all LG_{0p} modes, it is not practically relevant to use this mode family for energy scaling.

In this regard, the $LG_{\ell 0}$ family is much more interesting because of the scaling properties shown in Table 1, as previously identified [12,21]. In these works, the main argument used to perform experiments with the LG_{10} mode is that the Gouy phase multiplier in this case does not allow coupling to other $LG_{\ell p}$ modes. In contrast, e.g., using the LG_{20} mode results in a Gouy phase multiplier equal to 0 for coupling to the LG_{01} mode. However, as argued above, in this case, the amplitude of the coupling coefficient is zero because of conservation of the OAM. We therefore test this hypothesis and show the results of a simulation that uses the LG_{20} mode as an input, with a pulse energy of 1.35 mJ to match the spectral broadening of the benchmark Gaussian case. These results are shown in Fig. 5 and demonstrate almost perfect conservation of the LG_{20} mode, with 99% of the output energy contained in this mode at the output, at the same overall nonlinearity level. While the benchmark simulation done with a Gaussian beam corresponds to a ratio between the input peak power and the critical power of $P_{\text{peak}}/P_{\text{crit}} = 0.29$, the LG_{20} case corresponds to $P_{\text{peak}}/P_{\text{crit}} = 0.10$, which contributes to the very robust spatial stability.

B. Quasi-Collimated Cell

To further assess the scaling possibilities opened by the use of these modes, we perform simulations in a quasi-collimated MPC, a geometry that enables compact folding due to the fact that the stationary beam features an almost constant size throughout propagation [25]. The MPC parameters are $R = 25$ m and $L = 8.63$ m, with 11 roundtrips. The mirrors do not introduce any spectral phase, with a reflectivity of 99.5%. The input pulse is 1 ps long, with an energy of 8 mJ. These parameters match the experimental configuration described in Ref. [25], except for the gas nature and pressure: The MPC is filled with argon at a pressure of 1.2 bar, which is the maximum pressure that can be tolerated without introducing too much Kerr lensing perturbation to the propagation, and corresponds to $P_{\text{peak}}/P_{\text{crit}} = 0.55$.

In a first step, it is interesting to investigate the mode transfer properties of this collimated MPC over the first few passes when excited with a Gaussian beam, as was shown in Fig. 3 for the concentric case. Figure 6 shows the beam radius, on-axis B-integral, and modal energy fraction over the first four passes. In this geometry, the beam remains well into the Rayleigh range, and the Gouy phase accumulated by the Gaussian beam can be evaluated using Eq. (2) to be 0.86 rad. As a consequence, the rate at which the phase of the nonlinear coupling term between LG_{00} and LG_{01} slips per pass is much less than in the quasi-concentric case, and it takes several passes (in this case, four, because the accumulated Gouy phase per pass is a little over $\pi/4$) for the energy to flow back to the Gaussian mode. Because of this smaller phase mismatch, despite a lower B-integral per pass, the maximum fraction of energy coupled into the LG_{01} mode over the first four passes amounts to 6%.

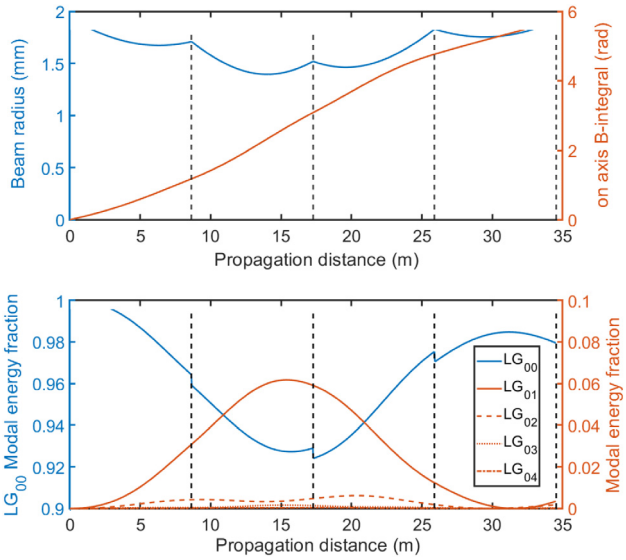

Fig. 6. (Top) Caustic and accumulated on-axis B-integral as a function of distance over the first four passes for the collimated MPC driven by a Gaussian beam. (Bottom) Energy fraction in the LG_{0n} modes. The dashed lines indicate the location of the cell mirrors.

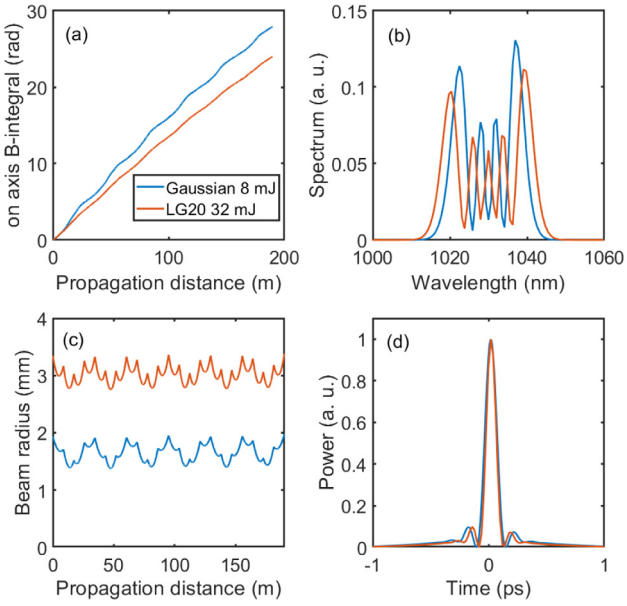

Fig. 7. Comparison of Gaussian and LG_{20} modes in the quasi-collimated MPC geometry. (a) Accumulated B-integral as a function of distance. (b) Output spectrum. (c) Root-mean square beam radius as a function of distance. (d) Compressed output temporal profile. The blue curves correspond to a Gaussian mode with 8 mJ, and the red curves correspond to a LG_{20} mode with 32 mJ.

As shown in Fig. 7, in the Gaussian case, propagation over the 11 roundtrips in this collimated MPC results in output pulses that can be compressed down to 115 fs, with negligible energy transfer (<1%) to higher-order spatial modes at the output. The tolerable peak B-integral per pass is smaller than for a quasi-concentric MPC [19] and amounts to 1.15 rad. Although nonlinear propagation perturbs the caustic, the fluence on the mirrors remains below 0.22 J/cm^2.

Propagation with the same MPC parameters is computed for a 32 mJ pulse in the LG_{20} mode. In these conditions, the fraction of energy contained in the LG_{20} mode at the output is again >99%. As shown in Fig. 7, the accumulated peak B-integral is slightly lower than in the Gaussian case, while the spatially averaged spectrum is slightly broader, resulting in a compressed pulsewidth of 96 fs. This is roughly in line with the nonlinear parameters provided in Table 1. Indeed, the 32 mJ energy was selected to yield a comparable spatially averaged spectral broadening to the Gaussian case considered. According to Table 1, this should happen for an energy equal to $8 \times (8/3) = 21$ mJ, determined by the ratio in effective area between these modes, but we observe that we need to increase the energy beyond this value to get a similar spectral broadening. A possible explanation for this is that, as the ratio of peak power to critical power increases, modifications to the linear caustic induced by Kerr lensing increase the spectral broadening compared to the expected value, as observed, e.g., in Ref. [26]. Because the ratio in critical power between these modes is 8, the LG_{00} is operated closer to the critical power than the LG_{20}, which causes this increase in energy that we need to make to get comparable broadening. In terms of peak B-integral, the ratio in input energy that should result in identical values is $2/e^2 = 3.7$, which is compatible with this analysis. At this energy level, the beam radius as a function of distance is also slightly perturbed by Kerr lensing, but the maximum fluence on the mirrors is 0.19 J/cm^2, comparable to the Gaussian case. This confirms the very promising potential of using Laguerre–Gaussian beams with a higher value of the angular order as the input condition to nonlinear MPCs for compression.

6. MULTIMODE BEHAVIOR IN THE NONLINEAR REGIME

We now confront arguments from the coupled-mode theory to numerical simulations in the case where the input spatial profile is a mix of two modes. We choose to launch a mix of LG_{00} and LG_{02} modes, with half the energy in each mode, a zero relative phase, and a total energy of 500 μJ in the quasi-concentric MPC described in Section 5.A. As a result, six nonzero source terms are driven by these two excited modes in Eq. (7). If we require in addition that the nonlinear coefficient Gouy phase multiplier is zero, each of these six terms results in efficient energy exchange with a single mode. More explicitly, the $LG_{00}LG_{00}^{*}LG_{00}$ and $LG_{02}LG_{02}^{*}LG_{02}$ terms self-couple to modes LG_{00} and LG_{02}, respectively, and are responsible for SPM. The $LG_{00}LG_{00}^{*}LG_{02}$ and $LG_{00}LG_{02}^{*}LG_{02}$ terms couple to modes LG_{02} and LG_{00}, respectively, and are responsible for cross-phase modulation and energy exchange between the two initially excited modes. The $LG_{00}LG_{02}^{*}LG_{00}$ term does not couple to a forward-propagating wave, and therefore it does not affect the propagation. Finally, the $LG_{02}LG_{00}^{*}LG_{02}$ couples out to the LG_{04} mode. As a consequence, a number of mechanisms prevents smooth accumulation of a spatially homogeneous nonlinear phase and a controlled spatial dynamics. Initially excited modes exchange energy, which modifies the spatial profile along propagation. Because they have different effective areas, they accumulate B-integral at different rates, which translates into a space-dependent spectrum, or an equivalently

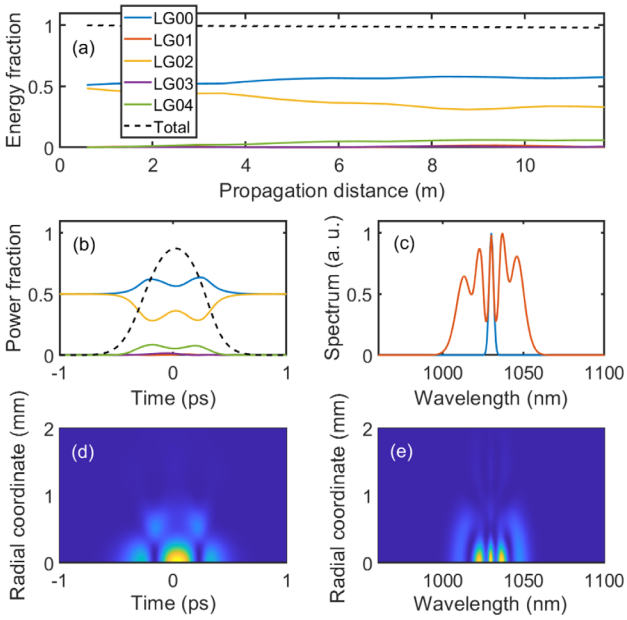

Fig. 8. (a) Modal content as a function of propagation distance in the quasi-concentric MPC excited with a mix of LG_{00} and LG_{02} modes. (b) Time-resolved modal content at the output. The dashed line indicates the normalized space-averaged temporal profile at the output. (c) Input (blue) and output (red) spatially averaged spectra. (d) Output spatio-temporal intensity. (e) Output spatio-spectral intensity.

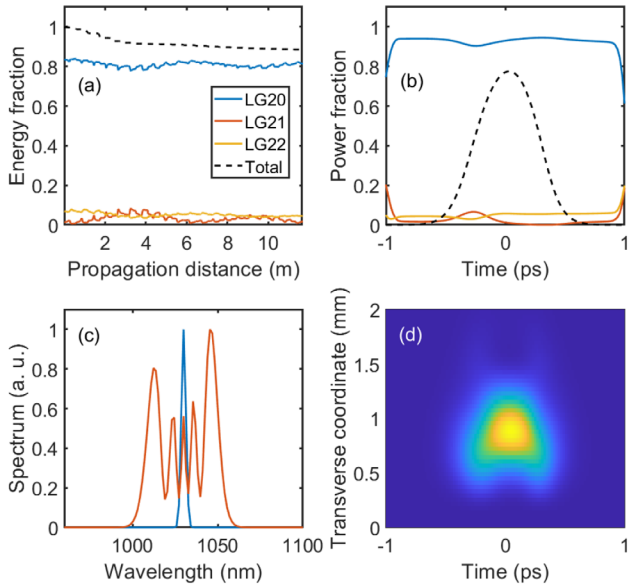

Fig. 9. (a) Modal content as a function of propagation distance in the quasi-concentric MPC excited with a nonideal LG_{20} mode. (b) Time-resolved modal content at the output. The dashed line indicates the normalized space-averaged temporal profile at the output. (c) Input (blue) and output (red) spatially averaged spectra. (d) Output spatio-temporal intensity.

time-dependent spatial profile or mode content. It is noteworthy that this property also results in a nonlinear correction to the phase-matching condition between each mode and the source terms, a well-known phenomenon in FWM processes. Finally, efficient energy transfer toward higher-order modes is permitted, in this case mainly to the LG_{04} mode.

The result of the simulation is shown in Fig. 8. The energy transfer between the two initially excited modes LG_{00} and LG_{02} is clearly observed. It is also verified that the initially nonexcited mode that gathers the most energy during propagation is the LG_{04} mode, with about 6% of the energy compared to less than 1% for the other modes that are monitored. The time-resolved mode projection shows that the spatial content is clearly time-dependent, which is also apparent in the spatio-temporal profile. The spatio-spectral profile also exhibits couplings, which result in a spatially averaged spectrum that significantly deviates from a typical SPM-induced spectrum, as a result of the nonlinear mode mixing and mode-dependent SPM. Instead of high-visibility spectral oscillations that are observed for single-mode SPM, the spatially averaged spectrum consists in the superposition of various modes with different B-integrals, washing out the spectral oscillations. Depending on the initial modal excitation, and overall nonlinearity, these observed phase-matched energy exchanges between modes can hinder efficient and high-fidelity pulse compression when using multimode fields such as a flat-top profile at the input.

From these observations, the question arises as to how pure a single higher-order mode should be in order to avoid these detrimental multimode effects. Although the answer to this question probably depends on multiple factors such as the level of nonlinearity, MPC geometry, and overall accumulated B-integral, we investigate a special case of practical importance. Returning to the results of Fig. 5 that correspond to propagation of a perfect LG_{20} mode in the quasi-concentric MPC, we simulate a more realistic situation where the LG_{20}-like mode is generated by inserting a vortex plate introducing a phase $\exp(j\ell\theta)$, $\ell = 2$, over a Gaussian beam. The waist of this Gaussian beam is increased by a factor $\sqrt{1+|\ell|}$ to maximize the fraction of energy coupled to the LG_{20} mode in this process [21]. The rest of the parameters are unchanged with respect to Fig. 5. In this situation, the field at the output is composed of 83.5% LG_{20}, 1.5% LG_{21}, 7% LG_{22}, with the remaining 8% in higher-order modes. This high spatial frequency content is due to the nonzero intensity at the center of the beam, over which a very quickly varying phase is applied.

Figure 9 shows the corresponding results. Over the first few roundtrips, the overall energy that propagates in the MPC decreases by $\approx 8\%$ because the high-frequency content is radiated out of the computation window and removed by the absorbing boundary condition of the simulation. Mild energy exchange is observed mostly between LG_{20} and LG_{21} modes, but this does not cause major changes in the intensity profiles. We think that the fast, small amplitude oscillations that occur at each mirror are a digital artifact, due to the projection operation upon the mode basis. At the output, the space-integrated spectrum remains very close to the case where a pure LG_{20} mode is excited. The spatio-temporal intensity exhibits weak spatio-temporal couplings, probably due to the different nonlinear phases seen by LG_{20} and LG_{22} modes, but the output beam remains reasonably well-behaved: The fraction of energy contained in the LG_{20} mode is 92%. For this particular case, the nonperfect single mode input condition does not prevent the use of a MPC to perform temporal compression.

7. CONCLUSION

To conclude, we have examined properties of the nonlinear propagation of higher-order- and multimode ultrashort wavepackets in MPCs. Considerations based on the couple-mode theory allow us to predict the energy transfer between modes when one or two modes are excited at the input. The use of higher-order $LG_{\ell 0}$ modes seems particularly interesting to scale the energy inside these systems. Indeed, all mode properties such as the effective area, maximum intensity, and critical power scale favorably, and coupling to higher-order modes is inhibited, at least at nonlinearity levels that are typically used for temporal compression.

However, guaranteeing that a single higher-order mode is excited at the input is important since the simultaneous excitation of several modes with the same angular order ℓ but a different radial order p results in possible phase-matched flow of energy toward other modes and significant spatio-temporal couplings at the output. As the azimuthal order ℓ increases, the ratio of energy between higher-order modes and the targeted $LG_{\ell 0}$ obtained by using a simple spiral phase plate on an initially Gaussian beam increases, and we expect lower compression fidelity. In this regard, more sophisticated and efficient mode conversion methods such as multiplane light converters [27,28] could prove useful.

MPCs have often been seen as a bulk implementation of optical fibers in the sense that they are quasi-waveguides, and their multimode properties also resemble the physics that has recently been explored in graded-index fibers, where the intermodal group velocity spread is small. The existence and/or observation of multimode optical effects such as beam cleaning [29], Rayleigh–Jeans condensation [30], or geometric parametric instability [17] is an open question, as well as the impact of other nonlinear phenomena such as Raman scattering on the spatial dynamics [31]. Another interesting question connected to this work is the behavior of bulk material-based nonlinear MPCs with respect to higher-order- or multimode beams. In this case, the physics is significantly changed by the fact that nonlinearity is not homogeneous, but rather localized in space.

Funding. Agence Nationale de la Recherche (ANR-21-CE30-0038-SHOTIME, ANR-24-CE92-0010-02 MILLSTREAMS); Université Paris-Saclay (PHOM ShapeNL).

Disclosures. The authors declare no conflicts of interest.

Data availability. Data underlying the results presented in this paper are not publicly available at this time but may be obtained from the authors upon reasonable request.

REFERENCES

1. J. Schulte, T. Sartorius, J. Weitenberg, *et al.*, "Nonlinear pulse compression in a multi-pass cell," Opt. Lett. **41**, 4511–4514 (2016).
2. M. Hanna, F. Guichard, N. Daher, *et al.*, "Nonlinear optics in multipass cells," Laser Photonics Rev. **15**, 2100220 (2021).
3. A.-L. Viotti, M. Seidel, E. Escoto, *et al.*, "Multi-pass cells for post-compression of ultrashort laser pulses," Optica **9**, 197–216 (2022).
4. Y. Pfaff, C. Forster, G. Barbiero, *et al.*, "Nonlinear pulse compression of a thin-disk amplifier and contrast enhancement via nonlinear ellipse rotation," Opt. Express **30**, 10981–10990 (2022).
5. N. Daher, X. Délen, F. Guichard, *et al.*, "Raman wavelength conversion in a multipass cell," Opt. Lett. **46**, 3380–3383 (2021).
6. N. Milosevic, G. Tempea, and T. Brabec, "Optical pulse compression: bulk media versus hollow waveguides," Opt. Lett. **25**, 672–674 (2000).
7. M. Hanna, L. Daniault, F. Guichard, *et al.*, "Nonlinear beam matching to gas-filled multipass cells," OSA Contin. **4**, 732–738 (2021).
8. M. Seidel, P. Balla, C. Li, *et al.*, "Factor 30 pulse compression by hybrid multipass multiplate spectral broadening," Ultrafast Sci. **2022**, 1–10 (2022).
9. S. N. Vlasov, E. V. Koposova, and V. E. Yashin, "Spectral broadening and compression of high-intensity laser pulses in quasi-periodic systems with Kerr nonlinearity," Quantum Electron. **42**, 989 (2012).
10. H. Cao, R. S. Nagymihaly, V. Chvykov, *et al.*, "Multipass-cell-based post-compression of radially and azimuthally polarized pulses to the sub-two-cycle regime," J. Opt. Soc. Am. B **36**, 2517–2525 (2019).
11. H. Cao, R. S. Nagymihaly, and M. Kalashnikov, "Relativistic near-single-cycle optical vortex pulses from noble gas-filled multipass cells," Opt. Lett. **45**, 3240–3243 (2020).
12. M. Kaumanns, D. Kormin, T. Nubbemeyer, *et al.*, "Spectral broadening of 112 mJ, 1.3 ps pulses at 5 kHz in a LG_{10} multipass cell with compressibility to 37 fs," Opt. Lett. **46**, 929–932 (2021).
13. L. G. Wright, W. H. Renninger, D. N. Christodoulides, *et al.*, "Nonlinear multimode photonics: nonlinear optics with many degrees of freedom," Optica **9**, 824–841 (2022).
14. C. Brahms and J. C. Travers, "Soliton self-compression and resonant dispersive wave emission in higher-order modes of a hollow capillary fibre," J. Phys. Photonics **4**, 034002 (2022).
15. M. Vimal, M. Natile, J.-F. Lupi, *et al.*, "Nonlinear post-compression of a hybrid vortex mode in a gas-filled capillary," Opt. Lett. **49**, 117–120 (2024).
16. M. Guer, M. Luttmann, J.-F. Hergott, *et al.*, "Few-cycle optical vortices for strong-field physics," Opt. Lett. **49**, 93–96 (2024).
17. K. Krupa, A. Tonello, A. Barthélémy, *et al.*, "Observation of geometric parametric instability induced by the periodic spatial self-imaging of multimode waves," Phys. Rev. Lett. **116**, 183901 (2016).
18. A. E. Siegman, *Lasers* (University Science Books, 1986).
19. M. Hanna, X. Délen, L. Lavenu, *et al.*, "Nonlinear temporal compression in multipass cells: theory," J. Opt. Soc. Am. B **34**, 1340–1347 (2017).
20. L. Sá and J. Vieira, "Self-focusing of multiple interacting Laguerre-Gauss beams in Kerr media," Phys. Rev. A **100**, 013836 (2019).
21. M. Kaumanns, "Generation of energetic femtosecond pulses at high average power," Ph.D. thesis (Ludwig Maximilan University Munich, 2020).
22. M. G. de Oliveira, L. J. Pereira, A. S. Santos, *et al.*, "Radial-angular coupling in self-phase-modulation with structured light," Phys. Rev. A **108**, 013503 (2023).
23. K. Tarnowski, S. Majchrowska, P. Béjot, *et al.*, "Numerical modelings of ultrashort pulse propagation and conical emission in multimode optical fibers," J. Opt. Soc. Am. B **38**, 732–742 (2021).
24. J. F. Ward and G. H. C. New, "Optical third harmonic generation in gases by a focused laser beam," Phys. Rev. **185**, 57–72 (1969).
25. A. Schönberg, S. Rajhans, N. Khodakovskiy, *et al.*, "Pulse energy scaling of post-compression using folded multi-pass cells," in *Conference on Lasers and Electro-Optics* (2024), paper SM4Q.6.
26. N. Daher, F. Guichard, S. W. Jolly, *et al.*, "Multipass cells: 1D numerical model and investigation of spatio-spectral couplings at high nonlinearity," J. Opt. Soc. Am. B **37**, 993–999 (2020).
27. J.-F. Morizur, L. Nicholls, P. Jian, *et al.*, "Programmable unitary spatial mode manipulation," J. Opt. Soc. Am. A **27**, 2524–2531 (2010).
28. N. K. Fontaine, R. Ryf, H. Chen, *et al.*, "Laguerre-gaussian mode sorter," Nat. Commun. **10**, 1865 (2019).
29. K. Krupa, A. Tonello, B. M. Shalaby, *et al.*, "Spatial beam self-cleaning in multimode fibres," Nat. Photonics **11**, 237–241 (2017).
30. H. Pourbeyram, P. Sidorenko, F. O. Wu, *et al.*, "Direct observations of thermalization to a Rayleigh–Jeans distribution in multimode optical fibres," Nat. Phys. **18**, 685–690 (2022).
31. R. Safaei, G. Fan, O. Kwon, *et al.*, "High-energy multidimensional solitary states in hollow-core fibres," Nat. Photonics **14**, 733–739 (2020).